Journal Name

RSCPublishing

ARTICLE

High finesse optical cavity coupled with a quartz-enhanced photoacoustic spectroscopic sensor

Cite this: DOI: 10.1039/xoxxoooooox

Pietro Patimisco[a], Simone Borri[b], Iacopo Galli[b], Davide Mazzotti[b], Giovanni Giusfredi[b], Naota Akikusa[c], Masamichi Yamanishi[d], Gaetano Scamarcio[a], Paolo De Natale[b], and Vincenzo Spagnolo[a]

Received ooth June 2014,
Accepted ooth xxxx 2014

DOI: 10.1039/xoxxoooooox

www.rsc.org/

An ultra-sensitive and selective quartz-enhanced photoacoustic spectroscopy (QEPAS) combined with a high-finesse cavity sensor platform is proposed as a novel method for trace gas sensing. We called this technique Intra-cavity QEPAS (I-QEPAS). In the proposed scheme, a single-mode continuous wave quantum cascade laser (QCL) is coupled into a bow-tie optical cavity. The cavity is locked to the QCL emission frequency by means of a feedback-locking loop that acts directly on a piezoelectric actuator mounted behind one of the cavity mirrors. A power enhancement factor of ~240 was achieved, corresponding to an intracavity power of ~0.72 W. CO_2 was selected as target gas to validate our sensor. For the P(42) CO_2 absorption line, located at 2311.105 cm^{-1}, a minimum detection limit of 300 parts per trillion by volume at a total gas pressure of 50 mbar was achieved with a 20 s integration time. This corresponds to a normalized noise equivalent absorption of $3.2 \cdot 10^{-10}$ $W \cdot cm^{-1}/Hz^{1/2}$, comparable with the best results reported for QEPAS technique on much faster relaxing gases. A comparison with standard QEPAS performed under the same experimental conditions confirms that the I-QEPAS sensitivity scales with the intracavity laser power enhancement factor.

Introduction

High resolution and high sensitivity spectroscopic techniques incorporating laser sources are key tools in gas monitoring and trace detection applications. They are nonintrusive, do not require sample preparation, provide real-time information and allow in situ monitoring or remote detection.[1, 2] By using mid-infrared (IR) laser sources it is possible to get access to strong fundamental vibrational bands, located in the molecular fingerprint spectral region between 4 μm and 12 μm, of a large number of gas molecules of fundamental and/or applied interest, allowing highly sensitivity and selectivity detections. Quantum cascade lasers (QCLs) provide complete coverage of this wide spectral region, and have demonstrated to be suitable for a large variety of spectroscopic techniques including frequency-modulation spectroscopy[3], cavity-enhanced absorption spectroscopy[4] (CEAS), cavity ring-down spectroscopy[5] (CRDS), photoacoustic spectroscopy[6] (PAS), and quartz-enhanced PAS[7] (QEPAS). The commercial availability of room temperature continuous-wave external cavity QCLs with wide tuning ranges (up to 200 cm^{-1}), high power and relatively narrow linewidth[8] enables both multi-component sensing and detection of broadband molecular absorbers.

Photoacoustic spectroscopy (PAS) is one of the most used spectroscopic techniques for trace gas sensing applications due to its high sensitivity and selectivity[6]. Energy deposited in the gas of interest via absorption of modulated optical radiation is converted to local heating by collisional processes, thereby creating a pressure wave (sound) in an acoustic cell. The photoacoustic signal is detected by sensitive microphones and its strength can be enhanced by modulating the excitation source at a frequency matching an acoustic resonance of the cell. A well-established variation of the conventional PAS is the QEPAS technique that was first reported in 2002[9]. This technique uses a mm-size piezoelectric quartz tuning fork (QTF) as an acoustic wave transducer operating in quadrupole mode. This, together with the high Q-factor and the ~32.7 kHz resonance frequency of the QTF provide immunity to environmental acoustic noise. Moreover, QEPAS have demonstrated a large dynamic range of up to nine orders of magnitude of the photoacoustic signal and its noise is ultimately limited by the fundamental Johnson thermal noise of the QTF[10]. Very recently, QEPAS combined with mid-IR QCL sources has demonstrated record sensitivities up to 50 part-per-trillion (ppt) concentration levels in 1 s lock-in time constant for SF_6 detection[11,12]. The intensity of the QEPAS signal is directly proportional to the power absorbed by the target species and thus the sensitivity varies linearly with the laser power. One viable way to increase the laser power can be the employment of power build-up approaches, like the one occurring in high-finesse optical cavities.

Very recently, we reported on the first realization of a novel spectroscopic technique combining QEPAS with CEAS, that we called intra-cavity QEPAS (I-QEPAS)[13], demonstrating CO_2 detection sensitivities in the parts per trillion (ppt) concentration range. We will report here a detailed description of the design and characterization of this innovative technique and its comparison with a standard QEPAS sensor operating in the same experimental

conditions. We will also provide a detailed discussion about the characteristics of the compact bow-tie four-mirror optical resonator developed for the I-QEPAS apparatus and the locking loop performances.

Experimental set-up

Within an optical cavity, light is reflected repeatedly by high-reflectivity mirrors, giving rise to a power enhancement proportional to the number of round-trips (enhancement factor) in correspondence to well defined frequency values (cavity resonance frequencies). The resonance frequencies occur every *c/L*, where *c* is the speed of light and *L* the round-trip length and the spectral separation between two consecutive resonances is the so-called free-spectral range (*FSR*). The quality of an optical resonator strongly depends on the cavity losses (including residual transmission or absorption by the mirrors) and it is measured by a parameter called finesse (*F*), which is defined as the ratio between the *FSR* and the resonance full-width at half maximum value $\Delta\nu$: $F = FSR/\Delta\nu$. The finesse can also be calculated by taking into account the total cavity losses per round trip, $1-\rho$, according to $F = 2\pi/(1-\rho)$. For ring cavities, a power enhancement factor *E* up to F/π can be obtained for perfect mode matching[4]. As a consequence, the higher the finesse (i.e. the mirror reflectivity), the larger is the power enhancement factor and the narrower is the resonance width. With mirror reflectivities > 99%, the cavity will easily have a series of evenly spaced, sharp resonances with linewidths even smaller than 10 MHz[14]. In CEAS setups, the laser wavelength has to be matched with one of the cavity resonances, and a proper locking between the laser frequency and the cavity resonance has to be implemented for spectral scans. Usually, two approaches are performed: i) part of the light exiting the cavity is fed back to the laser[15,16] (optical feedback); ii) the cavity length is adjusted in order to match the laser frequency. By using a closed-locking loop electronic circuit it is possible to force the laser and the cavity to be in resonance by acting on the cavity itself (typically on a piezoelectric actuator moving one of cavity mirrors)[14]. In this second approach, modulation techniques can be used to derive an electronic error signal that represents the deviations of the laser frequency from a given cavity mode. In this way, the laser is kept in resonance with the length of the cavity and a very high spectral resolution can be achieved if high reflectivity mirrors are used. Since high laser power is required for strong QEPAS signals, the use of optical cavities promises to significantly increase the sensitivity of the QEPAS technique according to the effective power enhancement factor. This factor strongly depends on the cavity finesse and on the quality of the mode matching between the laser and the cavity, that can be optimized by properly handling the beam geometry entering the cavity and by using a laser radiation with a linewidth comparable to or narrower than the cavity mode. Recently, free-running continuous-wave QCL linewidths of ~1 MHz or below were demonstrated in combination with low-noise stabilized current sources[17], and linewidths in the kHz range were demonstrated on QCL by frequency locking to sub-Doppler absorption lines[18] or by phase locking to a frequency comb referenced radiation[19]. In addition, when the laser mode matching to the TEM_{00} cavity mode is realized, an intra-cavity beam with an excellent spatial beam profile can be obtained, which is advantageous for a proper focalization of the beam between the prongs of the quartz tuning fork[12].
The experimental sensor platform is shown in Fig. 1.

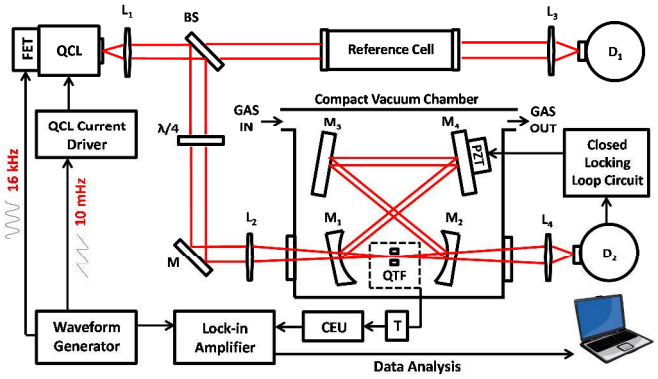

Fig.1 Schematic of the I-QEPAS apparatus. QCL: quantum cascade laser; FET: field-effect transistor; L: lens; BS: beam-splitter; D: detector; M: mirror; T: transimpedance amplifier; CEU: control electronic unit; QTF: quartz tuning fork.

The laser source is a room-temperature continuous-wave distributed-feedback QCL (Hamamatsu Photonics) emitting at 4.33 μm wavelength with a maximum power of 10 mW at 800 mA driving current. The QCL output radiation is collimated by a ZnSe lens (L_1) with a short focal length. A polarizing beam splitter transmits part of the laser beam (about 10% in power) towards a reference cell filled with pure CO_2. The beam that exits this cell is collected by a ZnSe lens (L_3) and detected by an HgCdTe liquid-N_2 cooled detector (D_1 in Fig. 1). The beam reflected by the beam splitter is focused into a bow-tie shaped optical cavity composed by 4 mirrors, two sphericals with radius of curvature of 30 mm (M_1 and M_2 in Fig. 1) and two planes (M_3 and M_4). The total cavity length (round-trip distance) is $L = 174$ mm. The laser beam-cavity optical coupling was realized by employing a CaF_2 plano-convex mode-matching lens (L_2) having a focal length of 100 mm. The coupling between the laser beam and the TEM_{00} optical mode of the cavity was verified by acquiring the laser beam profile coming out of the cavity with a pyroelectric camera placed behind M_2. M_4 is connected to a piezoelectric transducer (PZT) which allows a fine tuning of the cavity length up to ~10 μm. All four mirrors use YAG substrates, have a diameter of 0.5 inches and are coated with dielectric layers to reach a reflectivity of R = 99.9% at the laser wavelength and at 10 degrees angle of incidence. The decision of working with tilted mirrors was taken in order to avoid the strong feedback on the QCL induced by the radiation retro-reflected by the input mirror M_1. An InSb infrared detector (D_2 in Fig. 1) is placed after M_2 and collects the radiation exiting the cavity. Its output serves as error signal for the locking loop between the laser and the cavity. The QTF is mounted on a three-axis translator and is placed between M_1 and M_2. The estimated beam waist ($1/e^2$ radius) between the two spherical mirrors in these operating conditions (neglecting astigmatic distortions) is 60 μm, assuring a beam diameter well below the spacing between the two prongs of the QTF (~ 300 μm). The QTF acts as a piezoelectric acoustic transducer able to efficiently detect the pressure wave generated by non-radiative gas relaxation, which follows the laser absorption by the target gas mixture filling the cavity. We experimentally verified that all the intracavity beam power passes between the prongs of the fork without hitting it, which is a mandatory condition in order to reduce thermal noise and spurious background on the photoacoustic signal[10]. The resonator is housed into a vacuum chamber equipped with two anti-reflection coated CaF_2 windows for entrance/exit of the

light and filled with the target gas at selected pressures (see Fig. 1). The low-noise current driver is equipped with an input channel allowing for slow (<1 kHz) modulations for mode-hop-free frequency tuning of the laser. Faster modulations (up to tens of MHz) can be applied directly to the QCL chip by means of a field-effect transistor (FET). A custom built control electronics unit (CEU) is used to measure the electrical parameters of the QTF (dynamical resistance R, quality factor Q and resonant frequency f_0). The measured QTF resonance frequency is f_0 = 32,809 Hz, slightly depending on the gas pressure, and the quality factor Q exceeds 30,000 at operative pressure conditions (50 mbar). An electric resistance of 42.1 kΩ was measured, leading to a thermal noise level of 11.6 μV. The piezoelectric signal generated by the QTF was detected by a low noise transimpedance amplifier with a 10 MΩ feedback resistor, converted into a voltage signal and then demodulated by a lock-in amplifier.

Principle of operation of the I-QEPAS technique

The optical properties of the resonator were preliminarily estimated on the basis of the mirror reflectivity according to the equations described in the experimental section. We calculated a finesse of about 1570 by taking into account only the partial transmittivity of the mirrors as round-trip losses. By measuring the total length of the cavity, the free spectral range results: $FSR = c/L$ =1.725 GHz. Finally, the cavity mode FWHM can be estimated as the ratio between the FSR and the finesse: $\Delta\nu = FSR/F$ =1.1 MHz, comparable to the free-running laser linewidth. After alignment, the actual optical properties of the cavity can be precisely measured by recording the signal transmitted by mirror M_2. The operating temperature of the QCL was stabilized at 283 K and the injected current was linearly tuned by applying a slow voltage saw-tooth ramp to the current driver, in order to span an entire FSR. In Fig. 2 a recording of two consecutive transmission peaks (under vacuum conditions) is shown, and a zoom over a single resonance is shown in the inset.

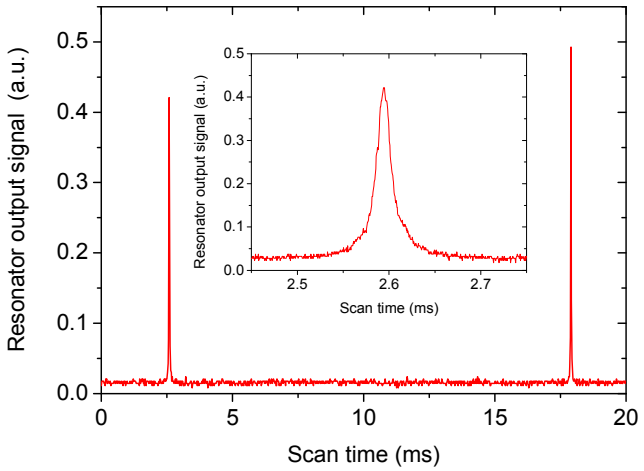

Fig.2 Cavity transmission spectrum acquired with the liquid-nitrogen cooled InSb detector, when a slow voltage saw-tooth ramp is applied to the QCL current driver and all four mirrors are fixed, under vacuum conditions. Inset: zoom over a cavity mode.

By knowing the FSR, the horizontal scale can be converted into frequency (MHz), and a Lorentzian fit of the cavity mode allows to measure its width: $\Delta\nu$ = 1.15 MHz, in good agreement with the estimated value. The measured finesse F of the optical resonator thus results to be F = 1505. According to cavity geometry, mirror reflectivities and the measured finesse, a power enhancement factor E = 240 was obtained.

In our experiments, we need to lock the resonance frequency of the cavity to the laser one during the slow linear scan. The simplest way is to adjust accordingly the cavity length by using the PZT via an electronic feedback signal. To generate a low noise error signal we add a sinusoidal frequency modulation (at the frequency $f_0/2$) to the laser radiation, so that the signal from the InSb detector demodulated at $f_0/2$ by a lock-in amplifier reproduces the first derivative of the resonator transmission signal, i.e. a dispersive error signal centered at zero. An electronic control loop processes the error signal by means of a proportional-integral operational amplifier module and closes the locking loop on the PZT, tuning the cavity length. Robust locking is possible thanks to the narrow linewidth and high intensity laser beam inside the resonator, which provides a low noise error signal. In Fig. 3 the cavity output in locked mode is shown (black curve), when a 0.1 Hz tuning triangular ramp (not shown in the picture) and the sinusoidal modulation at 16 kHz (red sinusoidal curve) are applied to the current driver.

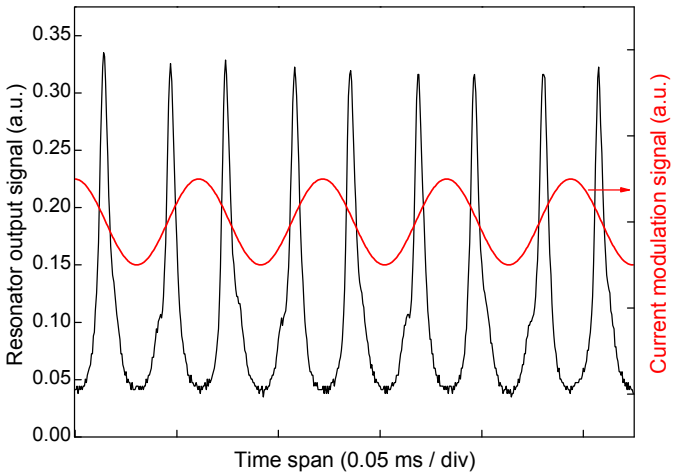

Fig.3 The cavity output signal (black curve) under vacuum conditions, acquired by the InSb detector in locking conditions when a 0.1 Hz tuning triangular ramp (not shown in the picture) and the sinusoidal modulation at 16 kHz (red curve) are applied to the QCL current driver.

The resonator output signal is not flat during the scan but it is characterized by a series of peaks at twice the frequency of the sinusoidal modulation. This behavior is expected if one considers that, the PZT response is not fast enough to follow the fast dither at 16 kHz. Thus, the slow locking loop is able only to keep the optical cavity resonant with the laser frequency at the *center* of the fast dither during the slow tuning ramp. Consequently, the locking loop acts as a mechanical chopper at 32 kHz (f_0) for the infrared light radiation in the cavity, forcing the resonator to follow the slow tuning ramp but not the fast dither. The overall effect is to produce an amplitude modulation on the intracavity radiation interacting with the gas sample and leading to the generation of an acoustic wave at the QTF resonance frequency f_0.

I-QEPAS sensor validation

I-QEPAS spectral scans were realized by stabilizing the temperature of the QCL at 283 K while the laser frequency was linearly tuned across the selected molecular transition by applying a slow voltage ramp to the laser. In addition, a sinusoidal dither at $f_0/2$ was applied to the QCL as described above, both for locking the cavity and for generating the intracavity acoustic wave at the QTF resonance frequency f_0. Due to the "chopping" effect of the cavity, our sensor works in amplitude modulation regime, and the I-QEPAS signal is obtained by demodulating the piezoelectric signal generated by the QTF at the same frequency f_0 with a lock-in amplifier.

To test our sensor we selected carbon dioxide (CO_2) as the target gas. CO_2 is the main product of combustion processes and human activities. Its monitoring has assumed a primary importance for global control of the environment and for industrial, medical and geophysical purposes. We targeted the $(00^01) - (00^00)$ P(42) roto-vibrational transition of CO_2 centered at 2311.105 cm^{-1} with a linestrength S = $4.749 \cdot 10^{-19}$ cm/mol (HITRAN units). The selected line is free from interference of common air constituents (such as H_2O, CO, N_2O and CH_4)[20]. We experimentally observed a strong absorption from ambient CO_2 in air, leading a significant attenuation of the laser beam along its open-air path (~ 30 cm) before entering the cavity. Therefore, the available power at the center of the absorption line was $P = 3$ mW before the input mirror, corresponding to an intracavity optical power of about $Pc = P \cdot E = 0.72$ W. Working in amplitude modulation regime, our sensor is affected by a non-negligible signal offset. The overall system response is the results of a sum of three components: i) an unwanted background due to acoustic signal (mostly due to the laser absorption by the windows and external acoustic disturbances); ii) a contribution due to laser absorption by ambient CO_2 in the optical path outside the cavity; iii) the I-QEPAS signal generated by the absorption of CO_2 in the pressure-controlled chamber. The background acoustic signal has a nearly wavelength-independent nature in the narrow spectral range corresponding to ~two times the CO_2 absorption linewidth. Whereas, the contribution to the absorption by ambient CO_2 in the air-path has a broad Lorentzian shape (if compared to the I-QEPAS signal), which can be estimated to have a 4.72 GHz full width at half maximum (FWHM). By acquiring background spectra with the optical cavity filled with pure nitrogen, we verified that the pure background signal can be fitted by a Lorentzian function (with the FWHM forced to the calculated value) plus a constant offset[13]. We consequently subtract the background components from all acquired spectra discussed in this work in order to extract the resulting I-QEPAS signal due to the gas sample filling the cavity.

In order to determine the best operating conditions, we studied the I-QEPAS signal dependence on the gas pressure and the laser modulation depth (induced by the sinusoidal dither). For this analysis a certified mixture of 860 part-per-billion (ppb) of CO_2 in pure nitrogen (N_2) was used. In Fig. 4a is reported the I-QEPAS peak signal as a function of the laser modulation depth at gas mixing pressure of 50 mbar. The peak signals were normalized to its maximum value. The results illustrate the influence of the laser modulation depth on the I-QEPAS signal. The region between 10 and 13 MHz appears quite flat, so we selected 10 MHz as the operating modulation depth. Using this modulation, we were able to completely scan the resonance of the cavity during each half period of the sinusoidal laser modulation. Figure 4b depicts the I-QEPAS signal amplitude as a function of the sample pressure at 10 MHz modulation depth. The gas pressure influences the QEPAS signal mostly because the Q-factor decreases at higher pressures, while the vibrational-translational (V-T) energy transfer relaxation rate is faster at higher pressures, resulting in more efficient sound production. Therefore, there is a trade-off value for the pressure, where the I-QEPAS peak signal reaches its highest value. In our experiments, this condition is obtained for a gas pressure of 50 mbar.

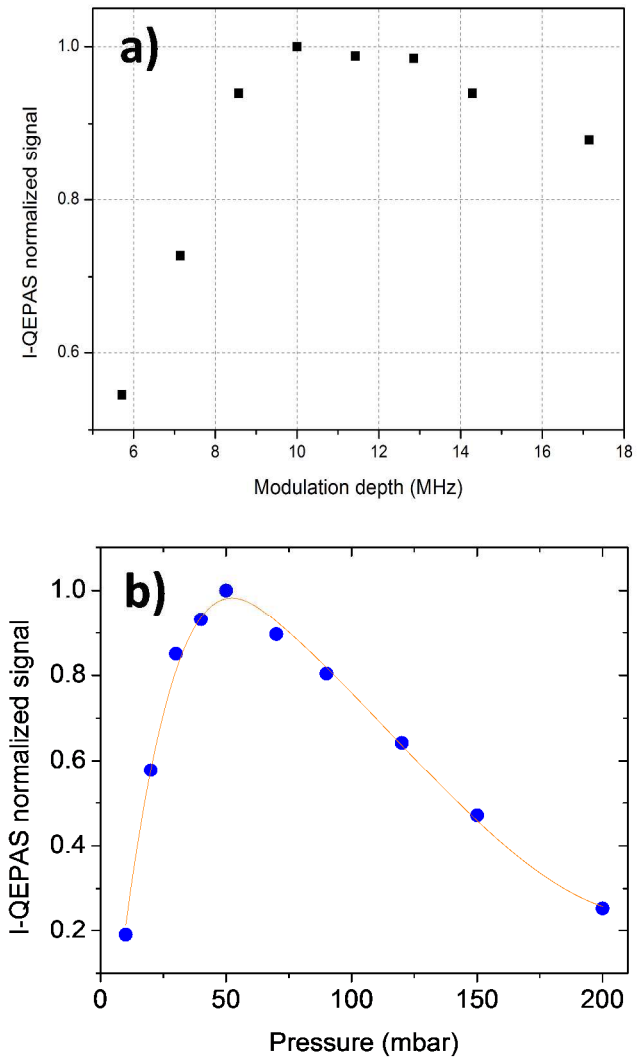

Fig.4 (a) I-QEPAS signal amplitude plotted as a function of the modulation depth for a certified mixture of 860 ppb of CO_2 in pure N_2 at a total gas pressure of 50 mbar. The conversion factor between the modulation amplitude (peak-to-peak, in volts) and the laser frequency span is 140 MHz/V, obtained by previous calibration of the driver modulation input on Doppler broadened molecular line. (b) I-QEPAS signal amplitude plotted as a function of total gas pressure with the same certified gas mixture and a modulation depth of 10 MHz. The solid line is a guide for eye.

For the sensor validation, different CO_2 concentrations in the 860 ppb – 50 ppb range were realized by diluting the calibration mixture of 860 ppb CO_2:N_2 in dry N_2. High-resolution I-QEPAS scans of a CO_2:N_2 mixtures with 410 ppb, 300 ppb, 170 ppb, 90 ppb and 50 ppb CO_2 concentrations acquired with a lock-in time constant of 1 s are shown in Fig. 5.

As expected I-QEPAS spectral scans do not show the 2nd derivative-like shape typical of 2*f* lock-in demodulation, but has the typical absorption-like profile of pure amplitude modulation detection. Considering the noise fluctuations of 3.5 mV (1σ value measured on the flat tails of the absorption lines) and the I-QEPAS peak signal of 170 mV at 50 ppb of CO_2 concentration, we can extract for our I-QEPAS sensor a 1σ detection limit of 1 ppb at 4s integration time.

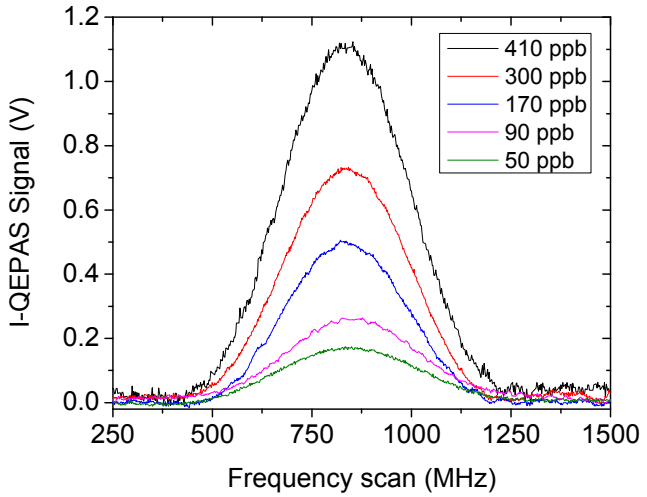

Fig.5 I-QEPAS Spectral scans of five representative CO_2 concentrations of 410 ppb, 300 ppb, 170 ppb, 90 ppb, and 50 ppb, obtained by diluting a certified mixture of 860 ppb of CO_2 in dry N_2. Scans are acquired with a modulation depth of 10 MHz, at a total gas pressure of 50 mbar and 4 second integration time (1 s lock-in time constant).

The response of the sensor was investigated by plotting the I-QEPAS peak signal as a function of the CO_2 concentration between 0 ppb (pure N_2) and 860 ppb. High CO_2 concentrations induce absorption losses inside the cavity comparable with those due to the mirror leakage. This reduces the cavity finesse *F*, and thus both the power enhancement factor *E* and the intracavity optical power. Since the photoacoustic signal is directly proportional to the available optical power between the two prongs of the QTF, all the experimental data were normalized with a factor defined as $\rho = F/F_0$, where F_0 is the finesse of the resonator in vacuum. This factor allows taking into account the decreasing enhancement factor (and thus the intracavity power) with increasing internal absorption losses given by higher CO_2 concentrations, as shown in Fig. 6. Experimental data and normalized experimental data are also shown in Figure 6.

I-QEPAS peak signals referred to low CO_2 concentrations (lower than 300 ppb) are not sensibly affected from the correction procedure confirming that our sensor works better at low gas target concentrations. For higher concentrations a standard QEPAS setup can be used or, alternatively, the correction procedure is mandatory.

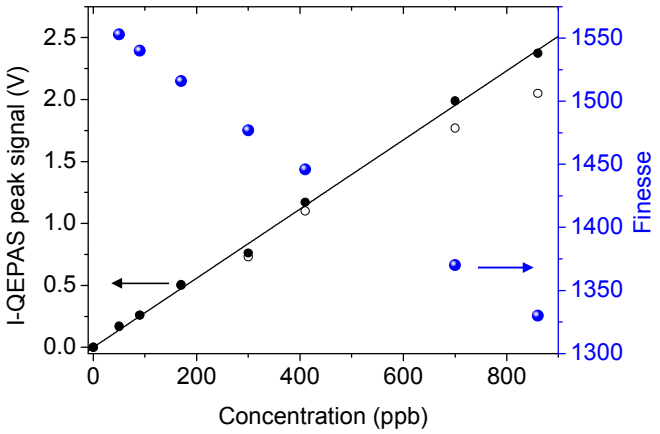

Fig.6 Calculated cavity finesse values (●) plotted as a function of the concentrations of CO_2 in the compact vacuum chamber. As the concentration of CO_2 grows, the finesse falls down due to the increase of CO_2 absorption losses in the cavity. I-QEPAS signals amplitude (○ symbols) as a function of the CO_2 concentration, and actual I-QEPAS signals amplitude (● symbols) normalized taking account the ρ factor. The solid line is the linear fit of the normalized QEPAS signals.

Comparison with standard QEPAS technique

In order to experimentally determine the enhancement in sensitivity induced by the optical power build-up approach, a set of measurements with the standard QEPAS approach was performed. The experimental setup is identical to that sketched in Fig. 1 except the optical cavity that here was removed. Now the collimated laser beam is focused directly between the prongs of the QTF. QEPAS spectral scans were performed by selecting the same absorption line and using a wavelength modulation (WM) approach and 2*f* detection: a sinusoidal dither at a frequency of $f_0/2$ was applied to the QCL through the FET controller and the QEPAS signal was demodulated at f_0 by means of a lock-in amplifier. The optimal sensor operating conditions were found to occur by working at a total gas pressure of 50 mbar and a modulation depth of 350 MHz. It worth noticing the strongly different modulation depths employed in QEPAS and I-QEPAS measurements. This is due to the different linewidths with which we have to deal in the two cases: the pressure-broadened molecular linewidth in QEPAS, the narrow width of the cavity mode in I-QEPAS setup. We determined the QEPAS sensor baseline by acquiring a complete scan with the cavity filled with pure N_2. We verified that in this case the spectroscopic signal had a flat zero background, as expected using the WM method. Different CO_2 concentrations in the 60–2.5 part-per-million (ppm) range were generated by diluting a certified mixture of 100 ppm of CO_2 in N_2. Spectral scans of a CO_2:N_2 mixtures with 56 ppm, 31 ppm and 11 ppm of CO_2 concentrations acquired with a lock-in time constant of 1 s are shown in Fig. 7.

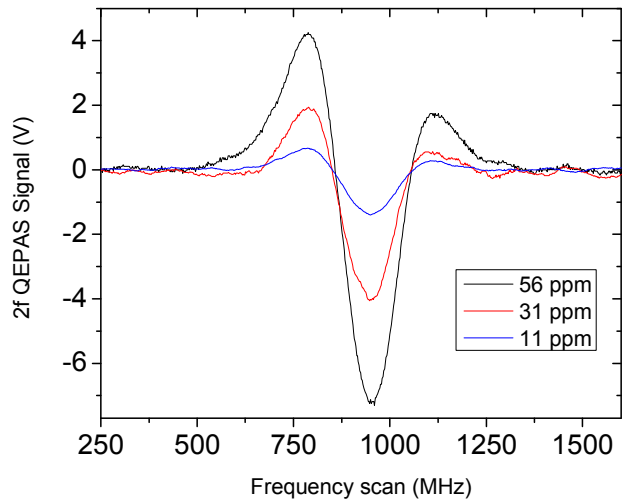

Fig.7 QEPAS spectral scans of a CO_2:N_2 mixtures with 56 ppm, 31 ppm and 11 ppm of CO_2 concentrations obtained by diluting a certified mixture of 100 ppm of CO_2 in dry N_2. The operating conditions are: gas pressure of 50 mbar, modulation depth of 350 MHz and lock-in time constant of 1 s (4 s integration time).

Note that the QEPAS spectrum has a 2nd derivative line-shape as expected but is slightly distorted. This distortion is exhibited through an asymmetry on both side of the spectrum around the peak position, and can be ascribed to a residual amplitude modulation contribution to a *2f* detection approach.[21] The linearity of the QEPAS peak signal as a function of the gas concentration was investigated and the calibration curve, plotted in Fig. 8, was obtained.

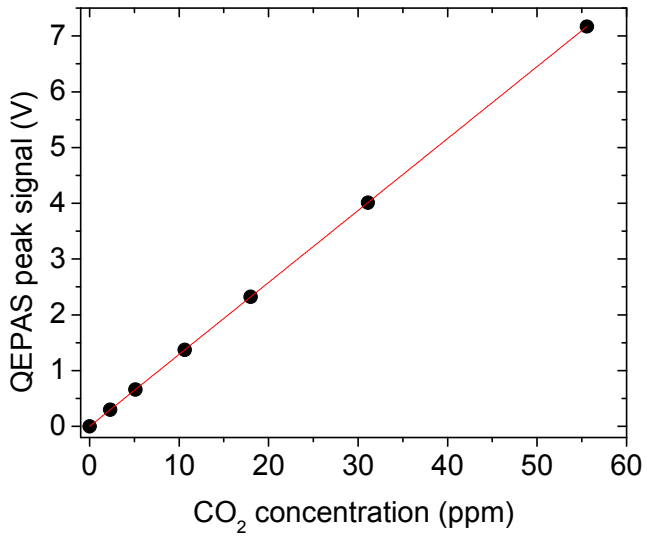

Fig.8 QEPAS signal as a function of the CO_2 concentration. The solid line is the best linear fit of the experimental data.

In order to determine the best achievable sensitivity of both the QEPAS and the I-QEPAS sensors we performed an Allan variance analysis measuring and averaging the signal at zero CO_2 concentration (pure N_2 in the chamber at 50 mbar) and with the laser frequency locked to the selected CO_2 absorption line. The comparison between the two Allan deviation plots are shown in Fig. 9. To verify the proportionality between the improvement in terms of sensitivity and the power enhancement factor we divided the QEPAS Allan plot by E = 240.

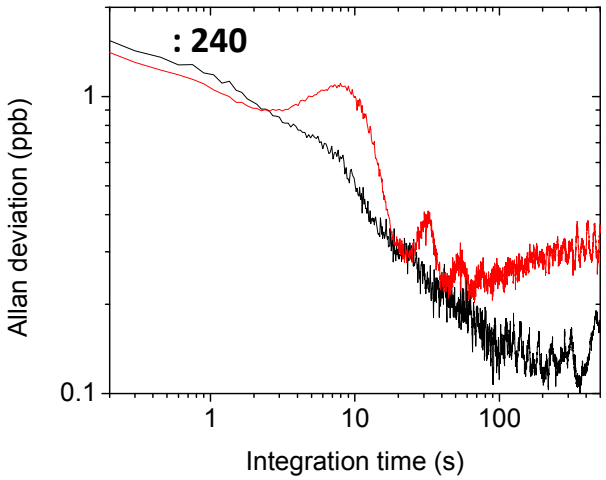

Fig.9 Comparison between Allan deviation plots in ppb CO_2 concentrations, obtained for I-QEPAS (red curve), and standard QEPAS (black curve), as a function of the integration time. For the sake of comparison, the QEPAS Allan plot has been divided by the power enhancement factor $E = 240$.

The comparison shows that after this rescaling the two curves almost overlap. The peaks (at ~8 s, 30 s and 50 s) in the I-QEPAS Allan deviation can be attributed to mechanical instabilities of the cavity and oscillations of the locking loop. The long term drift which marks the difference between the two curves from ~60 s on is probably due to thermal drifts of the cavity, which causes small fluctuations of the mirror positions and consequently of the beam waist. This produced a detectable effect on the QTF thermal noise. This effect can be canceled out by adopting proper temperature stabilization of the whole cavity, thus leading to improved sensitivities for longer integration times. For the QEPAS sensor at 20 s integration time we extract a 1σ minimum detectable concentration limit of 72 ppb, corresponding to α_{min}=3.3 $\cdot 10^{-6}$ cm^{-1} and a NNEA of 7.5 $\cdot 10^{-8}$ $W \cdot cm^{-1}/Hz^{1/2}$. At the same integration time, for the I-QEPAS sensor we estimated a 1σ equivalent concentration of 300 ppt, corresponding to a minimum absorption coefficient α_{min} = 1.4 $\cdot 10^{-8}$ cm^{-1} and a normalized noise equivalent absorption (NNEA) of 3.2 $\cdot 10^{-10}$ $W \cdot cm^{-1}/Hz^{1/2}$. These results confirm the achievement of a sensitivity enhancement factor for the I-QEPAS sensor, with respect to the standard QEPAS, corresponding to the power enhancement factor.

Conclusions

The architecture and performance of a novel ultra-highly sensitive, selective and real-time gas sensor called I-QEPAS based on mid-IR QCL and QEPAS detection in an optical power buildup cavity were described. We used a 4.3 μm DFB QCL that emits a maximum power of 3.0 mW in a continuous-wave operating mode. A highly efficient injection of the QCL light into the cavity was achieved, leading to an intra-cavity laser power of ~ 0.7 W. The capability of automatically maintaining the cavity frequency locked to the laser frequency was demonstrated by means of home-made built electronic circuit. A 1σ minimum detection limit of 300 ppt was achieved for an integration time of 20 s using an interference-free CO_2 absorption line, corresponding to a NNEA of 3.2·10^{-10} W·cm-

$^{1}/Hz^{1/2}$. The improvement in terms of sensitivity with respect to conventional QEPAS setup (operating under the same conditions of molecular linewidth, pressure and laser output power) results to be equal to the power enhancement factor occurring in the optical resonator. This demonstrates the validity of our approach, which pushes I-QEPAS among the most sensitive cavity-based techniques as ICOS or CRDS when fast relaxing gases are used. Further improvements in sensitivity can be in principle achieved with resonators with higher finesse, provided that suitable narrow-linewidth radiation is available. Moreover, since a bare QTF was used as acoustic detection module in our setup, further improvements are expected by adding metallic organ-pype micro-resonators to the photoacoustic detection module.

Notes and references

[a] *CNR-IFN UOS Bari and Dipartimento Interateneo di Fisica, Università e Politecnico di Bari, via Amendola 173, 70126 Bari, Italy*
[b] *CNR-INO UOS Sesto Fiorentino and LENS, via Carrara 1, 50019 Sesto Fiorentino FI, Italy*
[c] *Development Bureau Laser Device R&D Group, Hamamatsu Photonics KK, Shizuoka 434-8601, Japan*
[d] *Central Research Laboratories, Hamamatsu Photonics KK, Shizuoka 434-8601, Japan*

1. M. Ebrahim-Zadeh, M. and I. T. Sorokina: Mid-Infrared Coherent Sources and Applications (Springer, Houten, 2007).
2. M. Jahjah, W. Jiang, N. P. Sanchez, W. Ren, P. Patimisco, V. Spagnolo, S. C. Herndon, R. J. Griffin, and F. K. Tittel, *Opt. Lett*, 2014, **39**, 957-960.
3. S. Borri, S. Bartalini, P. De Natale, M. Inguscio, C. Gmachl, F. Capasso, D. L. Sivco, and A. Y. Cho, *Appl. Phys. B*, 2006, **85**, 223-229.
4. G. Gagliardi and H. P Loock: Cavity-Enhanced Spectroscopy and Sensing (Springer, London, 2014).
5. I. Galli, S. Bartalini, S. Borri, P. Cancio, D. Mazzotti, P. De Natale, and G. Giusfredi, *Phys. Rev. Lett.*, 2011, **107**, 270802.
6. A. Elia, P. M. Lugarà, C. Di Franco, and V. Spagnolo, *Sensors*, 2009, **9**, 9616-9628.
7. P. Patimisco, G. Scamarcio, F. K. Tittel, and V. Spagnolo, *Sensors*, 2014, **14**, 6165-6206.
8. G. Wysocki, R. Lewicki, R. F. Curl, F. K. Tittel, L. Diehl, F. Capasso, M. Troccoli, G. Hofler, D. Bour, S. Corzine, R. Maulini, M. Giovannini, and J. Faist, *Appl. Phys. B: Lasers Opt.*, 2008, **92**, 305-311.
9. A. A. Kosterev, Y. A. Bakhirkin, R. F. Curl, and F. K. Tittel, *Opt. Lett*, 2002, **27**, 1902-1904 (2002).
10. A. A Kosterev, F. K. Tittel, D Serebryakov, A. L. Malinovsky, and I. Morozov, *Rev. Sci. Instr.*, 2005, **76**, 1-9.
11. V. Spagnolo, P. Patimisco, S. Borri, G. Scamarcio, B. E. Bernacki, and J. Kriesel, *Opt. Lett.*, 2012, **37**, 4461-4463.
12. V. Spagnolo, P. Patimisco, S. Borri, G. Scamarcio, B. E. Bernacki, and J. Kriesel, *Appl. Phys. B: Lasers Opt.*, 2013, **112**, 25-33.
13. S. Borri, P. Patimisco, I. Galli, D. Mazzotti, G. Giusfredi, N. Akikusa, M. Yamanishi, G. Scamarcio, P. De Natale, and V. Spagnolo, *Appl. Phys. Lett.,* 2014, **104**, 091114.
14. R. D. Van Zee and J. P. Looney: Cavity-Enhanced Spectroscopies (Academic Press, San Diego, 2002).
15. M. Hippler, C. Mohr, K. A. Keen, and E. D. McNaghten, *J. Chem. Phys.*, 2010, **133**, 044308.
16. A. Kachanov, S.Koulikov, and F. K. Tittel, *Appl. Phys. B: Lasers Opt.*, 2013, **110**, 47-56.
17. S. Bartalini, S. Borri, I. Galli, G. Giusfredi, D. Mazzotti, T. Edamura, N. Akikusa, M. Yamanishi, and P. De Natale, *Opt. Express,* 2011, **19**, 17996-18003.
18. F. Cappelli, I. Galli, S. Borri, G. Giusfredi, P. Cancio, D. Mazzotti, A. Montori, N. Akikusa, M. Yamanishi, S. Bartalini, and P. De Natale, *Opt. Lett.*, 2012, **37**, 4811-4813.
19. I. Galli, M. Siciliani de Cumis, F. Cappelli, S. Bartalini, D. Mazzotti, S. Borri, A. Montori, N. Akikusa, M. Yamanishi, G. Giusfredi, P. Cancio, and P. De Natale, Appl. Phys. Lett. 2013, **102**, 121117.
20. L. S. Rothman, I. E. Gordon, Y. Babikov, A. Barbe, D. Chris Benner, P. F. Bernath, M. Birk, L. Bizzocchi, V. Boudon, L. R. Brown, A. Campargue, K. Chance, E. A. Cohen, L. H. Coudert, V. M. Devi, B. J. Drouin, A. Fayt, J. M. Flaud, R. R. Gamache, J. J. Harrison, J. M. Hartmann, C. Hill, J. T. Hodges, D. Jacquemart, A. Jolly, J. Lamouroux, R. J. Le Roy, G. Li, D. A. Long, O. M. Lyulin, C. J. Mackie, S. T. Massie, S. Mikhailenko, H. S. P. Müller, O. V. Naumenko, A. V. Nikitin, J. Orphal, V. Perevalov, A. Perrin, E. R. Polovtseva, C. Richard, M. A. H. Smith, E. Starikova, K. Sung, S. Tashkun, J. Tennyson, G. C. Toon, V. G. Tyuterev, and G. Wagner, *J. Quant. Spectrosc. Radiat. Transfer*, 2013, **130**, 4-50.
21. P. Patimisco, S. Borri, A. Sampaolo, H. E. Beere, D. A. Ritchie, M. S. Vitiello, G. Scamarcio, and V. Spagnolo, *Analyst*, 2014, **139**, 2079-2087.